nature materials

INSIGHT | REVIEW ARTICLES

PUBLISHED ONLINE: 20 DECEMBER 2016 | DOI: 10.1038/NMAT4676

Energy conversion approaches and materials for high-efficiency photovoltaics

Martin A. Green* and Stephen P. Bremner

The past five years have seen significant cost reductions in photovoltaics and a correspondingly strong increase in uptake, with photovoltaics now positioned to provide one of the lowest-cost options for future electricity generation. What is becoming clear as the industry develops is that area-related costs, such as costs of encapsulation and field-installation, are increasingly important components of the total costs of photovoltaic electricity generation, with this trend expected to continue. Improved energy-conversion efficiency directly reduces such costs, with increased manufacturing volume likely to drive down the additional costs associated with implementing higher efficiencies. This suggests the industry will evolve beyond the standard single-junction solar cells that currently dominate commercial production, where energy-conversion efficiencies are fundamentally constrained by Shockley–Queisser limits to practical values below 30%. This Review assesses the overall prospects for a range of approaches that can potentially exceed these limits, based on ultimate efficiency prospects, material requirements and developmental outlook.

Reports of the first efficient silicon solar cells in 1954[1] stimulated calculations of ultimate photovoltaic efficiency[2,3] and its dependence on the semiconductor bandgap (E_g). Calculating current-generation limits in a short-circuited cell is uncomplicated: each incident photon of energy above E_g is assumed to create one carrier that flows in the external circuit (Fig. 1a). Assigning fundamental limits to the open-circuit voltage (V_{OC}) is more problematic. Initial approaches estimated bounds[2,3] using Shockley's semiconductor p–n junction theory[4], combined with optimistic extrapolations of relevant material properties.

Shockley and Queisser[5] found an elegant solution to this difficulty. Noting solar cells must absorb sunlight strongly, they realized the optimal material properties would be related to those of ideal black bodies, at least for energies above E_g. Unbiased in the dark, good cells would receive and emit largely ambient temperature black-body radiation. Emitted photons of energy above E_g overwhelmingly originate from radiative recombination of electrons in the semiconductor conduction band with valence-band holes, as the strongest optical process at such energies. Photons generated in this way would have various fates, such as being reabsorbed or totally-internally-reflected at surfaces, but the number emitted is readily quantified by integrating the ambient temperature black-body photon spectrum above E_g.

With a voltage V across the cell (Fig. 1a), Shockley's p–n junction theory[4] shows that carrier concentration near the junction increases exponentially with qV/kT (where k is Boltzmann's constant, T is absolute temperature and q is electronic charge, with kT/q, the 'thermal voltage', equal to 26.69257 mV at 25 °C). Intuitively, Shockley and Queisser realized that, for good cells, similar enhancements throughout active volumes would correspondingly increase recombination rates. Hence, the number of photons emitted by good cells under voltage would be the above-bandgap thermal equilibrium emission enhanced by this exponential factor.

Single-junction cells

Calculating Shockley–Queisser (SQ) limits follows simply from the above insight. For limiting performance, all cell recombination will be radiative. The current that supports this recombination is equal to q times the emitted photon-flux, thus allowing calculation of the open-circuit voltage V_{OC}, the current–voltage curve and the limiting efficiency[5]. The limits for standard single-junction cells and the factors that influence these are described below.

Shockley–Queisser limits. Figure 1b shows limits calculated versus cell bandgap (or, more correctly, the absorption threshold, which is often smaller than E_g, when effects such as excitonic and phonon-assisted absorption are considered). Also shown are the highest experimental results[6], plotted versus energy absorption threshold. Since there is no unique way of determining this threshold, it was chosen for the plotted data as the photon energy, where experimental cell photon-to-electron external quantum efficiency, EQE_{pe}, increases to half-peak value at long wavelengths.

Two crystalline materials, Si and GaAs, have demonstrated efficiency above 25%, with assorted crystalline, polycrystalline and thin-film materials demonstrating efficiency clustered around the 21–22% range. A gap follows to the 10–15% range, where several other materials can be found.

Three loss categories cause experimental performance to fall below SQ limits: (1) collection losses, including photon reflection or absorption in poorly responding cell regions; (2) non-radiative recombination occurring together with radiative, decreasing output voltages, particularly for poor-quality materials and interfaces; (3) electrical losses, including cell series- and shunt-resistances. Losses (1) and (3) depend on cell-design specifics. Loss (2) can be quantified for any experimental cell by calculating its external radiative efficiency[7] (ERE), which is defined as the fraction of net recombination when the cell is open-circuited that is radiative. (This is closely related to the electron-to-photon EQE when measured as a light-emitting diode (LED)). Because SQ theory assumes 100% ERE, ERE determines how closely an experimental cell approaches the ideal.

Figure 1c shows cell energy-conversion efficiency versus ERE for a range of photovoltaic materials. For crystalline III–V materials, ERE can be as high as 32.3% for the record 28.8%-efficient GaAs cell. For silicon, ERE is lower (0.1–2.2%) and constrained to values well below 100%, as intrinsic non-radiative Auger recombination is stronger than radiative recombination[8,9]. Spanning the silicon ERE values are the polycrystalline chalcogenides, copper indium

Australian Centre for Advanced Photovoltaics, School of Photovoltaic and Renewable Energy Engineering, University of New South Wales, Sydney 2052, Australia. *e-mail: m.green@unsw.edu.au

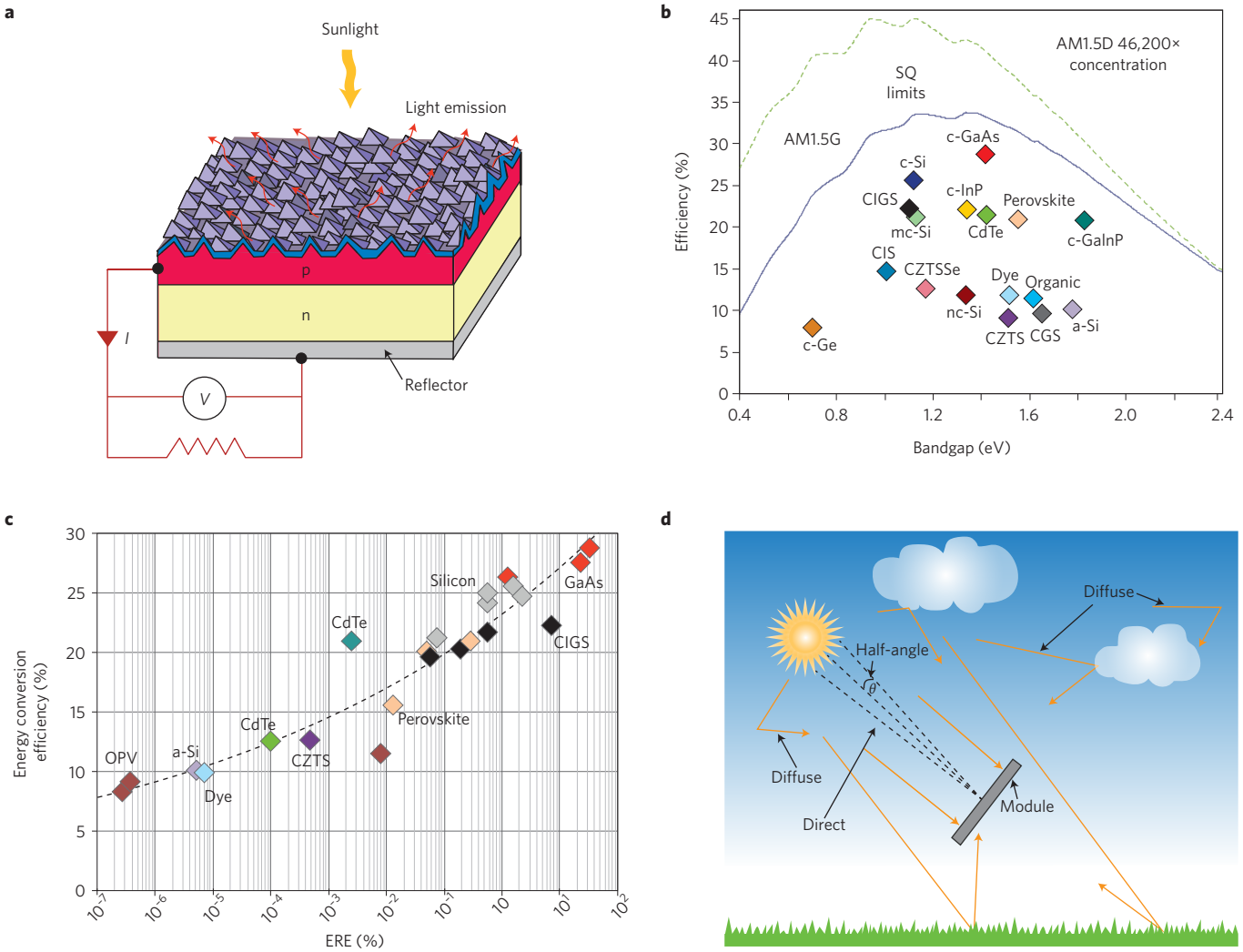

Figure 1 | Light absorption and emission, SQ limits, experimental energy-conversion efficiencies, radiative efficiencies and sunlight incident angles. **a**, Light absorption and emission from a solar cell under load. **b**, SQ energy-conversion efficiency limits under global sunlight (AM1.5G) versus energy absorption threshold (solid line), highest experimental values for various materials (data points) and limits for direct AM1.5D sunlight conversion under maximal concentration of 46,200 suns (dashed line), all at a cell temperature of 25 °C. Limits for other concentration ratios lie roughly geometrically intermediate between the solid and dashed lines, such that the curve for a concentration of 215 suns would lie around halfway between the two. **c**, Energy-conversion efficiency versus ERE for various experimental cells. **d**, Angular effects in solar energy conversion, showing direct and diffuse solar components, minimum acceptance angle and ground reflection effects. Data taken from refs 6,7.

gallium selenide (CIGS) and recently emerging perovskites. Next come other chalcogenides, CdTe and CZTSS ($Cu_2ZnSnS_ySe_{4-y}$), followed by dye-sensitized amorphous silicon and organic photovoltaic (OPV) cells. Organic LEDs have high values of electron-to-photon EQE because they are designed differently to their OPV counterparts[10], with LED-like design perhaps explaining one outlier in Fig. 1c — an organic photovoltaic cell with modest conversion efficiency despite reasonable ERE. The other outlier, a CdTe cell with 21% efficiency despite low ERE, is explained by high-quality processing, which gives a good fill-factor and photogenerated carrier collection.

The original SQ theory has been extended by two refinements. One is to include stimulated emission, which allows accurate treatment of the relationship between cell V_{OC} and E_g. The original theory predicts $V_{OC} > E_g/q$ under some conditions[11] (small E_g, strong illumination and low T), with the refinement limiting V_{OC} to E_g/q for ideal black-body cells (not necessarily for other cells[12]). The extended stimulated-emission formulation was first mentioned by Ross[13], extended by Würfel[14], and recently discussed analytically[15]. The second refinement relates light emission from practical cells to black-body emission[16]. In one of the semiconductor device field's surprising reciprocal relationships, emission from an actual cell, with some provisos, equals that from the black-body ideal at each wavelength and voltage, except multiplied by EQE_{pe} at that wavelength when used as a solar cell[16]. (The same relationship also applies to LEDs, although this is possibly not as well-known or exploited in that field.)

Concentrated sunlight. One way to exceed original SQ limits is to focus sunlight. The current in a short-circuited cell increases linearly with photon flux, whereas V_{OC} increases nearly logarithmically, thus giving a superlinear increase in power. The concentrator acceptance half-angle θ (Fig. 1d) determines[17] the maximum possible sunlight concentration (in air) of $1/\sin^2\theta$. At its mean distance, the Sun subtends a half-angle of 0.2665° at the Earth's surface[12], which corresponds to a maximum concentration of 46,200 suns.

The dashed line in Fig. 1b shows the limiting efficiency when the reference AM1.5D (air mass 1.5, direct illumination) spectrum is concentrated by this factor.

We note the potentially large gain in efficiency here, although some caution is needed. Only direct sunlight can be concentrated effectively and calculated efficiency relates only to this component, with incident diffuse sunlight — a large component of terrestrial sunlight[18] — simply neglected. Because standard photovoltaic reference spectra[19] are clear-sky spectra, 90% of sunlight in the standard AM1.5G (air mass 1.5, global illumination) spectrum is direct. Converting this with more than 11% relatively higher efficiency would increase output. However, high air mass, cloudy, hazy or overcast conditions all increase the diffuse fraction, thus increasing this required margin. Additionally, optical and resistive losses are more significant under concentration. Concentrators must also track the Sun's position, with this being optional in non-concentrating systems. On the plus side, concentration reduces the importance of cell costs by reducing cell area, thereby providing opportunities for the early introduction of advanced, high-efficiency concepts such as those discussed below.

It is worth noting that direct sunlight can be converted with high efficiency while simultaneously exploiting diffuse light, as suggested by Goetzberger, who described the use of a common scheme[12] in which a Fresnel lens array focuses direct sunlight onto high-efficiency concentrator cells. However, the space between concentrator cells is filled with low-cost cells, which convert diffuse light (similarly for direct light misdirected by lenses).

Acceptance angle. Similar gains can be obtained without concentration, in principle, by restricting cell acceptance angles so that cells convert light only from a limited directional range[20,21]. A non-concentrating Sun-tracking cell could absorb all direct sunlight if its acceptance half-angle θ equalled that subtended by the solar disc (Fig. 1d), with large values of EQE within the associated cone. If the cell reflected all light outside this cone, it would not emit at such angles (EQE = 0). In principle, emission would be reduced by $\sin^2\theta$, with limiting efficiencies identical to the highest in Fig. 1b (dashed line).

In this case, diffuse light also need not be wasted, as cell emission is strongly concentrated near the absorption edge. Light outside the acceptance cone could be accepted provided the associated energy absorption threshold is around 300 meV higher, which is feasible because diffuse light is relatively stronger at blue wavelengths[22]. Dielectric antireflection coatings become more reflective at longer wavelengths because the incidence angle increases, which suggests possible practical implementations[20,23].

Although the limiting efficiency is identical to that under concentration, non-radiative recombination becomes much more significant. Regardless of non-radiative recombination rates (hence ERE), concentration to 1,000 suns ideally increases V_{OC} by around 180 mV ($= (kT/q)\ln(C)$) at fixed cell temperature, with a concentration (or angular restriction) ratio of $C = 1{,}000$. However, if a smaller acceptance angle is used to reduce light emission by a factor of 1,000, this voltage gain occurs only for ideal cells where ERE = 1. For smaller values of ERE, the gain becomes $(kT/q)\ln\{C/[C - (C - 1)\mathrm{ERE}]\}$, which approaches zero as ERE $\rightarrow$ 0. Even for the highest experimental ERE to date (32.3%), V_{OC} would increase by only 10 mV, thus restricting gains to <1% under favourable assumptions, with this restriction not always emphasized in the literature[24,25].

Benefits can also accrue from increasing — rather than decreasing — acceptance angle. Substantial sunlight falls on the rear of a solar panel (Fig. 1d), either as diffuse sunlight or sunlight reflected from clouds, ground or other posterior structures. For fixed arrays, direct sunlight strikes panel rears on summer mornings and/or evenings. If panel acceptance angle is increased to accommodate both hemispheres, SQ limits decrease slightly due to the doubling of emission and the radiative recombination supporting it. However, energy output can increase by as much as 20–30%, particularly with high ground reflection[26,27].

Temperature. Solar cell efficiency decreases with increasing temperature. At 0 K, calculating SQ limits simplifies[14] because $V_{OC} = E_g/q$. Performance decreases approximately linearly to the 25 °C values in Fig. 1b. In the field, solar modules normally heat to temperatures that reflect their nominal operating cell temperature[28] — typically 44 °C, the temperature reached in an open-circuit configuration under 800 W m^{-2} illumination at an ambient temperature of 20 °C and with 1 m s^{-1} wind. This temperature rise decreases output by 5–12%, depending on the technology[28,29].

Heat losses from modules occur by convection, often wind-assisted, and by radiative transfer to sky and ground[28,29]. As well as receiving sunlight from various directions (Fig. 1d), modules emit and receive thermal radiation from these directions, in addition to SQ luminescent radiation. Most incident radiation comes at shorter wavelengths — below 4 μm — whereas at longer wavelengths module thermal radiation exceeds that received.

A module with ideal thermal design strongly absorbs above-bandgap photons while reflecting sub-bandgap photons over the wavelength band extending to 4 μm, in which more photons are absorbed than emitted, with modules here ideally reflective for all incident angles. An atmospheric window of 8–13 μm allows heat-sinking to cold space[30–32] rather than to ambient, so strong absorption and hence emission in this band is desirable. Even with hemispheric emission through a perfect window, only 133 W m^{-2} can be dissipated this way at 20 °C, with experimental demonstrations reaching 40 W m^{-2} (ref. 30).

Sub-ambient module temperatures are therefore feasible only for ultrahigh conversion efficiencies, at the upper limits discussed below. Less efficient devices are constrained to operating temperatures linked to sky, ambient and ground temperatures. The ideal module fully absorbs above the bandgap, fully reflects at intermediate wavelengths extending to 4 μm, and fully absorbs at longer wavelengths[32]. Standard modules approximate this ideal because low-iron glass coversheets become absorbing beyond wavelengths of 4 μm (ref. 33), although improvements such as the use of micrometre-sized, pyramidal-texturing of top glass surfaces may help in this regard[32]. Interestingly, these features have been used in high-performance modules, but to improve reflection and angular response rather than thermal performance[34].

Multijunction cells

One early suggestion — the most practical to date — involved improving efficiency beyond SQ limits, even before these limits were known, by steering different wavelength bands of sunlight to cells of appropriate bandgap for efficient conversion. Two schemes were originally suggested[35], either using filters to direct different wavelengths to appropriate cells (Fig. 2a), or, more elegantly, stacking cells on top of one another, arranged by bandgap to provide automatic filtering (Fig. 2b). The first approach has been used effectively in concentrators[36], whereas the second may be sufficiently low-cost to be suitable for 'one-sun', unconcentrated sunlight use, as stacking can be monolithic, with cells series-connected to produce simple two-terminal devices.

Early work extended the SQ approach to the analysis of such schemes[37,38]. One important issue, particularly as radiative limits are approached, is the treatment of radiative coupling between cells (Fig. 2b). Although coupling can reduce sensitivity to variations in sunlight spectra, the highest efficiency occurs when coupling is suppressed[39]. Figure 2 shows the corresponding limiting efficiency versus energy absorption threshold of the lowest-bandgap cell in a

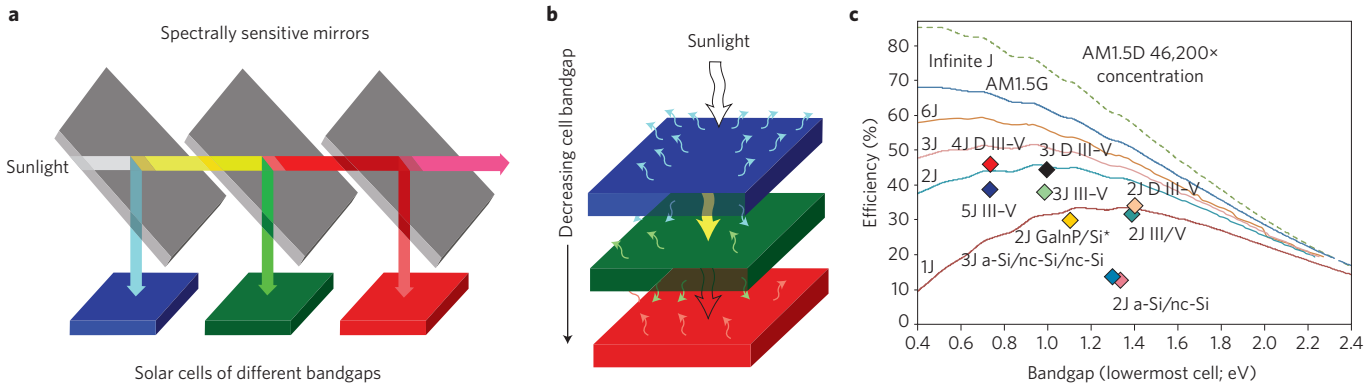

Figure 2 | Multiple-junction cells, efficiency limits and highest experimental results. a, Spectral splitting approach, in which filters are used to direct different wavelength bands in sunlight to appropriate cells. **b**, Stacked tandem cells, showing light transmission and radiative coupling. **c**, Limiting conversion efficiencies of various series-connected stacked tandem cells as a function of the energy absorption threshold of the lowermost cell and the number of cells in the stack (solid lines). Also shown (dashed line) is the limiting efficiency for a stack containing an infinite number of cells under maximal concentration (46,200 suns). Results for infinite cell numbers under other concentrations would be approximately geometrically intermediate between the upper AM1.5G and the dashed curve. Data points show the highest experimental efficiencies for different cell technologies under both unconcentrated (AM1.5G) and concentrated (AM1.5D) sunlight, with the number of junctions and cell materials also indicated. 3J, three-junction cells; D, concentrator cells under direct sunlight; *, mechanically stacked four-terminal device. All other devices are two-terminal monolithic devices. Data taken from ref. 6.

series-connected stack. Solid lines show the case of AM1.5G illumination, with a limiting efficiency of 68.0% for stacks that involve essentially infinite cell numbers, for lowermost cell thresholds of <0.5 eV. Stacks with finite cell numbers can approach this limit, as cell numbers increase.

Monolithic tandem cells have been most successfully implemented in the III–V material system, with record 38.8% efficiency measured under unconcentrated sunlight (AM1.5G) for a five-junction device[40] that involves cells fabricated on GaAs and InP wafers and then subsequently bonded together. The best two- and three-junction results are 31.6% and 37.9%, respectively, again using III–V semiconductors[41,42]. Another successful implementation has been in the thin-film amorphous-silicon (a-Si) and related nanocrystalline-silicon (nc-Si) system. Although efficiencies are much lower in these systems than in III–V material devices because of a more marginal material quality, they are appreciably higher than related single-junction devices. An AM1.5G efficiency of 13.6% has been reported for a triple-junction a-Si/nc-Si/nc-Si cell[43], compared with 10.2% and 11.8% for the best a-Si and nc-Si devices, respectively[44,45].

Increasing sunlight concentration (or restricting cell acceptance angle) increases efficiency limits, with the dashed line in Fig. 2c showing the infinite cell limit under maximal AM1.5D concentration. A maximum of 86.0% is possible when the lowermost cell bandgap approaches zero. Best experimental results are 46.0% at a concentration of 508 suns for a four-junction wafer-bonded cell[46], with efficiencies of 44.4% and 34.1% for three- and two-junction cells[42,47], respectively, again all using III–V semiconductors.

Considering likely photovoltaic evolutionary paths, it has been argued[48] that a key challenge is the search for a low-cost thin-film cell that can be deposited onto silicon or other commercial cell technologies to form high-efficiency tandem cells, with much present interest in perovskite/silicon tandem cells. Even triple-junction cells in this material system may be feasible, although substantial improvements in perovskite cell stability are essential before practical application is possible. Unconfirmed efficiencies above 20% have been reported[49,50], although poor stability is likely hindering independent confirmation. Similarly, using tandem stacks to supercharge other commercial technologies, such as CdTe and CIGS, would boost efficiency to levels that might eventually become mandatory to maintain competitiveness in the future.

Sub-bandgap absorption

A significant loss in standard cells is the wastage of sub-bandgap photons. One early suggestion for tackling this issue was the use of mid-gap states to capture such photons in a two-step absorption process (Fig. 3a)[51]. In their original paper[5], Shockley and Queisser suggested that analysing this problem using the SQ approach would show no benefits, with similar conclusions made in subsequent studies[52]. The proposal of a related multiple-absorption-threshold device — the multiple-quantum-well cell[53] (Fig. 3b) — which involves carrier photogeneration in lower-bandgap quantum-well regions and subsequent thermal escape to the higher-bandgap host material, stimulated work that clarified the basic thermodynamics of the two-step absorption process.

Associated thermodynamic constraints were resolved by extending SQ concepts to the related intermediate-band cell[54] (Fig. 3c). The corresponding device equivalent circuit for schemes of Fig. 3a–c is shown in Fig. 3d, where the rectangular circuit elements represent SQ-type cells.

Under concentrated sunlight, the efficiency limit approaches that of a three-cell tandem (Fig. 3e), as the parallel connection of Fig. 3d is not unduly restrictive. Energy wastage by absorbing high-energy photons in excitations possible with lower-energy photons must be avoided. Correlating the absorption strength for each excitation with its energy threshold or, alternatively, finite bandwidths for both valence and conduction bands, are two suggested strategies for avoiding such wastage[12].

The parallel connection becomes more restrictive under one-sun operation, as the combined voltage from elements C1 and C2 drops twice as rapidly with decreasing illumination as from element C1, thereby inhibiting a good voltage match. Importantly, efficiency can be improved if the defect level energy relaxes after occupation by an electron to a state that does not communicate radiatively with the band from which it originated (Fig. 3a), or, alternatively, if there is a 'ratchet' band with similar properties to which electrons can relax, in the case of intermediate-band devices (Fig. 3e). Benefits can be significant. For a silicon cell with ERE = 0.3%, introducing defects with ERE = 1% for transitions between the defect and either band increases the calculated efficiency from 26.7% to 32.0% with defect relaxation, assuming appropriate photon use[55]. Without relaxation, an optimally located defect with otherwise identical properties would reduce the efficiency to 18.4%, thus justifying earlier

pessimism regarding impurity photovoltaics[5,52]. Unfortunately, no defects with the required properties have yet been demonstrated.

For quantum-well cells (Fig. 3b), the conclusion is that fundamental improvements are only possible if carrier excitation from wells involves particles that are not in equilibrium with the lattice[56]. Examples are solar photons or hot phonons, which have higher effective temperature than the lattice. Even without such involvement, the quantum-well concept has proved to be useful because the additional well-region materials offer flexibility in bandgap and lattice-spacing control. Quantum-well cells that exploit these advantages briefly held the efficiency record for single-junction concentrator cells[57].

Intermediate band and impurity photovoltaic principles can be extended to multiple bands or defect levels[50]. The number of allowed transitions increases quickly, as do constraints on allowed energies, thereby sometimes restricting improvements even in ideal cases[58,59]. Attempts to implement intermediate-band devices in III–V and other material systems have not been particularly successful[60]; significant challenges remain for this approach, despite large potential gains.

Photon wavelength manipulation

Because the mismatch between photon energy and cell bandgap is a key contributor to relatively modest SQ limits, a generic approach for improving efficiency is to manipulate sunlight prior to conversion. Luminescent concentrators and photon up- and down-converters are key examples, as is thermophotovoltaics, which we discuss below as a thermal approach.

Figure 4a shows the principles of a luminescent concentrator[61,62]. Dye molecules or quantum dots impregnated into glass or plastic sheets absorb solar photons and subsequently re-emit them at lower energies in a narrow energy range close to the absorption threshold, but in random directions. A reasonable fraction will be totally-internally-reflected on striking surfaces of the embedding sheet and, through successive surface reflections, will be guided to the edges. Solar cells along these edges then convert the narrow-bandwidth light with high efficiency.

An appealing feature of luminescent concentrators is that they can concentrate both direct and diffuse sunlight. Analysing losses in practical systems can be complex, but high-level analysis of idealized systems produces an interesting result[63]. If a spectrally sensitive omnidirectional reflector — a 'hot mirror' — is placed along the top surface of the luminescent sheet so that all light below a certain energy threshold is reflected[64] (with the rear surface covered by a standard reflector), the limiting efficiency equals the SQ limit, with E_g replaced by the top-surface reflection threshold[63].

The expected good performance of a concentrator arises because the limiting efficiency decreases only slowly as the ratio of cell area to aperture area decreases, reaching more than 30% for geometric concentrations above 100 times. The situation is even better for cells with non-ideal properties. For a silicon cell with ERE = 0.24% and a conventional efficiency limit of 25.7%, an only slightly lower efficiency of 23.9% is calculated[63] in an ideal fluorescent concentrator at a geometric concentration of around 200 times.

A hot mirror is essential for such performance, although it is challenging to implement. Without a hot mirror efficiency falls rapidly with increasing geometric concentration, even under ideal conditions[63]. The most efficient experimental device lacks a hot mirror and is only 7.1% efficient at a geometric concentration of 2.5 times[65]. Efficiency can be improved, in principle, by stacking sheets with different absorption thresholds[62], but the luminescent approach does not seem conducive to high efficiency; its benefits may lie instead in attractive aesthetics[66].

A second spectrum-manipulation approach is photon up-conversion (Fig. 4b)[67]. In this scheme, photons with energy below E_g reach the rear up-converter and excite electrons to a higher energy

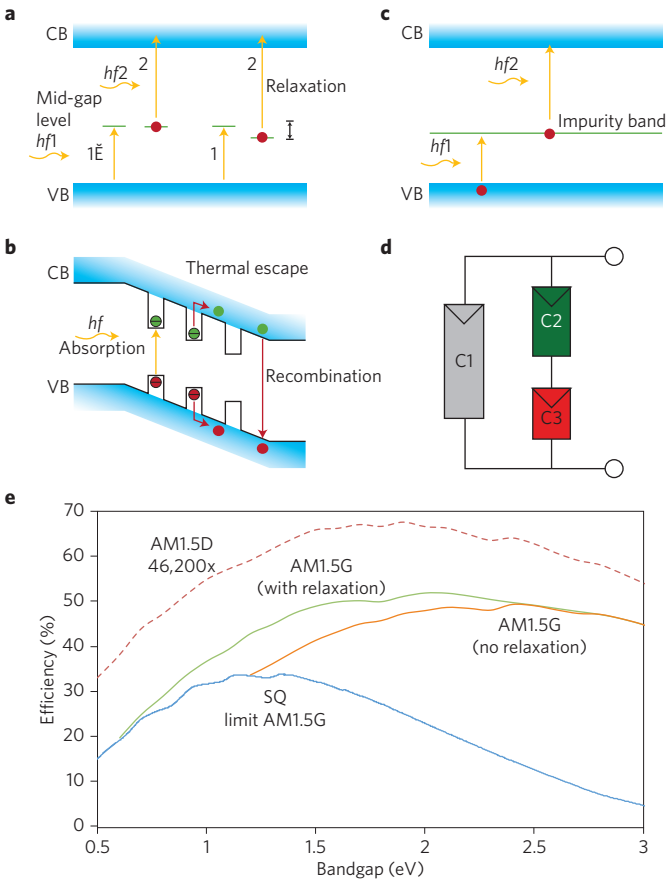

Figure 3 | Sub-bandgap absorption processes, equivalent circuit and limiting efficiencies. a, Excitation from the valence band (VB) to the conduction band (CB) through a mid-gap defect level, both without (left) and with (right) defect energy level relaxation. **b**, Quantum-well solar cell showing carrier generation by low-energy photons in quantum wells, with subsequent escape to the higher-bandgap host material. **c**, Solar cell in which an intermediate band is present, such as when impurities are present in sufficient quantities to cause overlapping between isolated states. **d**, Equivalent circuit that is common to sub-bandgap absorption approaches. The boxes indicate SQ-like cells, with box length representing the value of the cell's energy absorption threshold. **e**, Limiting efficiency under unconcentrated AM1.5G sunlight with and without energy relaxation (solid lines), achieved by relaxing to a 'ratchet band' in the case of intermediate-band cells[113]. The dashed line shows results under maximally concentrated AM1.5D radiation, where relaxation makes no significant difference.

through a two-step process similar to excitations in impurity photovoltaic and intermediate-band cells. Instead of being collected, the excited electrons relax to their ground state and thus emit a high-energy photon that is absorbed upon re-entering the cell.

The equivalent circuit for a two-step rear up-converter is shown in Fig. 4c. Efficiency increases appreciably under one-sun operation only if the intermediate state relaxes during the two-step excitation. This allows SQ elements C3 and C4 (Fig. 4c) to drive element C2 strongly into forward bias, thereby increasing its emission. Efficiency limits under unconcentrated sunlight (Fig. 4d) show substantial gains for all bandgaps, with a peak efficiency close to that of optimal three-cell tandems (Fig. 2c), as the equivalent circuit suggests.

The main experimental difficulty has been low radiative efficiency for practical up-converters — generally well below 1%. One suggested improvement[68] is the use of semiconductor up-converters (Fig. 4e).

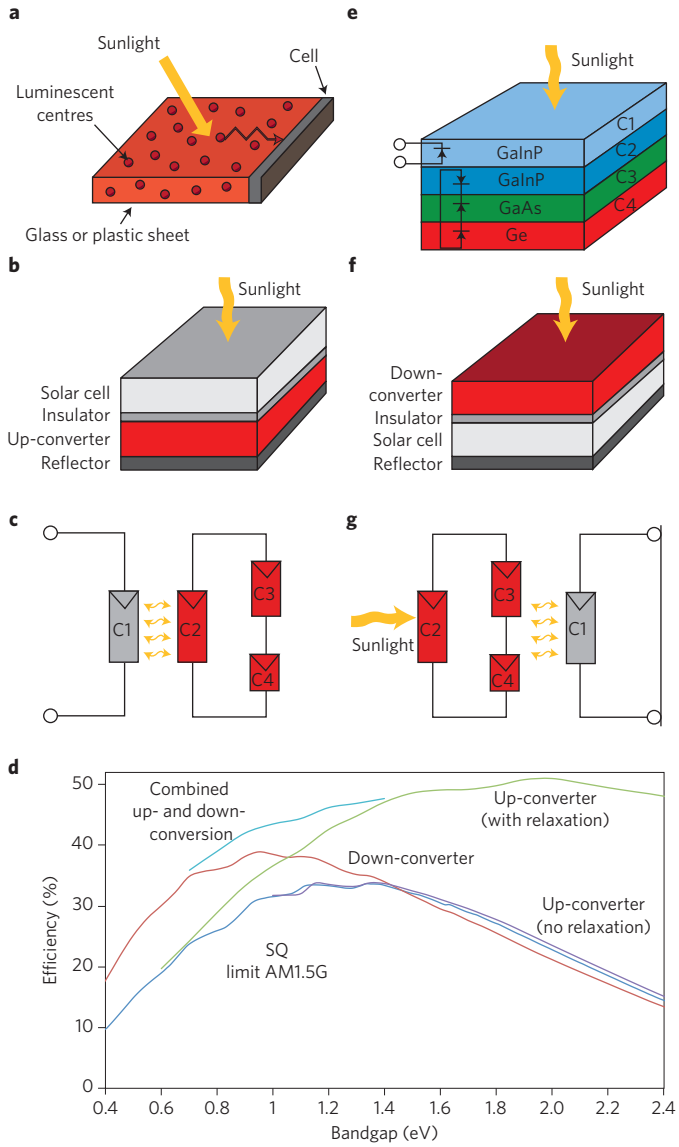

Figure 4 | Photon wavelength manipulation using luminescent concentrators and photon up- and down-conversion. a, Luminescent concentrator containing quantum dots or dye molecules impregnated into a glass or plastic sheet. Light is absorbed and re-emitted at a longer wavelength with high quantum efficiency, after which it can be collected by cells along the edge of the sheet. **b**, Photon up-conversion. Photons of energy below the cell absorption threshold pass through the cell and are absorbed in a rear up-converter, where two (or more) combine to produce a single higher-energy photon that can be converted by the cell. **c**, Equivalent circuit for the up-conversion process. **d**, Limiting efficiency for photon up- and down-conversion when combined under unconcentrated sunlight (AM1.5G). Energy relaxation of the intermediate state is critical for high efficiency in this case, as indicated. A refractive index of 3.6 was assumed for the down-converter calculations[61]. **e**, Proposed implementation of rear up-converter using III–V cells[60]. **f**, Photon down-conversion. A single high-energy photon is absorbed in a down-converter prior to incidence on the cell, resulting in the subsequent emission of two (or more) lower-energy photons. **g**, Equivalent circuit for the down-conversion process.

In this system, current in the GaInP top cell is boosted by emission from the underlying GaInP cell, which is driven by absorption in the two lowermost smaller-bandgap cells. Although the limiting efficiency is close to that of a three-cell tandem, its spectral tolerance is higher[68]. This approach may also eliminate current-mismatch losses that result from the low Ge bandgap in present triple-junction tandem cells on Ge substrates[36].

Down-conversion[69], in contrast, exploits the excess energy of high-energy photons. If a photon with energy more than $2E_g$ is intercepted before absorption, it can ideally double its carrier-generation potential by converting to two lower-energy photons. A possible front-surface configuration is shown in Fig. 4f, with an equivalent circuit in Fig. 4g. For cells with band-absorption characteristics (as is the case for some organic cells), rear-surface location is also feasible[69].

High-energy photons absorbed in element C2 generate sufficient voltage to drive elements C3 and C4 into forward bias, thus emitting photons that are then absorbed by the main cell. Because the bandgaps of elements C1, C3 and C4 are all similar, the scheme involves essentially two different bandgaps and has efficiencies comparable to those of two-cell tandems. The largest gains are obtained when the bandgap of C1 is small (Fig. 4d).

Down-conversion quantum efficiencies above 100% have been demonstrated experimentally[70,71] although challenges remain in applying this technique to photovoltaics. A semiconductor down-converter could be implemented using III–V devices in a manner similar to the up-converter of Fig. 4c, although only modest efficiency gains are expected compared with single-junction devices. Even with quantum efficiencies below 100%, practical benefits can accrue. Organic encapsulants in standard modules generally need protection from ultraviolet radiation. Absorbing ultraviolet photons in glass coversheets and down-shifting could be a useful strategy in this regard, particularly for cells with a poor ultraviolet response[70].

Because up- and down-conversion favour large and small bandgaps, respectively, there is benefit, in principle, in combining both for cells with mid-range bandgaps (Fig. 4d).

Multiple carriers per photon

SQ limits assume each absorbed photon produces a single carrier in the external circuit. Early semiconductor photodiodes demonstrated multiple-carrier generation by using high-energy photons[72], which becomes energetically feasible once the photon energy exceeds $2E_g$. Multiplication occurs through impact-ionization (Fig. 5a), which prompted the early suggestion of this approach for improving efficiency[73].

Analysis using SQ methodology produces interesting insights[74]. If multiple electrons/photons are introduced as a generation process, the inverse-recombination process — two electron–hole pairs recombining to give a single photon — must also be included to avoid thermodynamic inconsistencies. There has been much recent interest in multiple-exciton generation (MEG) in quantum-confined cells[75], although the high-level analysis remains unchanged. There is obviously a strong connection with down-conversion, which suggests links to two-cell tandems. Similar benefits would also apply if MEG were combined with up-conversion.

Ideally the quantum yield (number of electron–hole pairs per absorbed photon) would have the staircase property approached in Fig. 5c for large values of the parameter P. P is formally defined — perhaps obscurely — as the ratio of energy loss from multiple-particle generation (k_{MEG}) to that from other processes (k_{cool}) (Fig. 5b), at an energy twice the threshold for multiple-particle generation. Simple theory[72] gives a square-law dependence of this ratio with energy above this threshold, where the threshold energy equals $(2 + 1/P)E_g$. More modest experimental performance is seen than that given by the ideal staircase, although data are well characterized by finite P values.

Experimentally, P ranges from well below 1 for bulk materials to a peak of around 10 for PbSe nanorods[76]. Corresponding efficiency limits under non-concentrated AM1.5G sunlight (Fig. 5d) show that P values above 10 are required for gains over SQ limits,

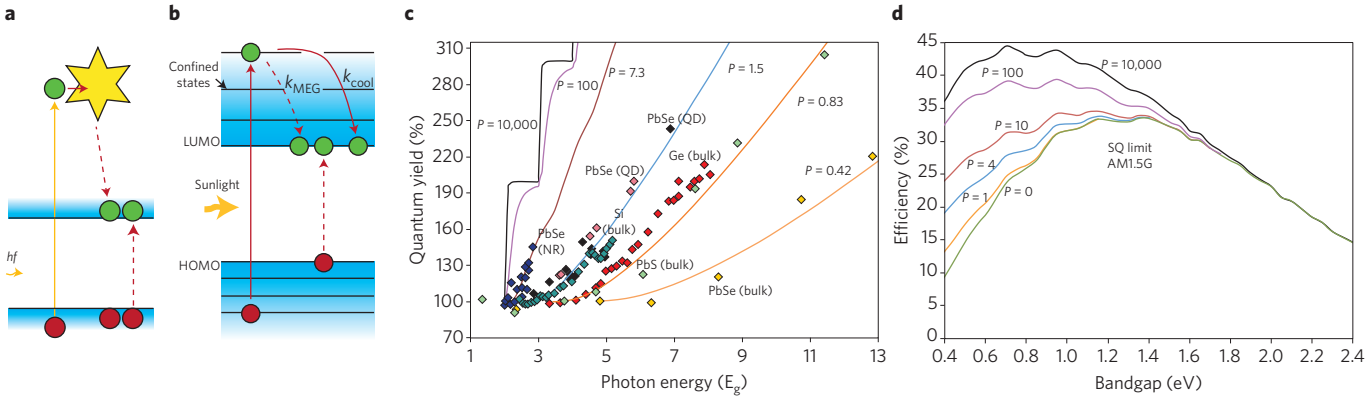

Figure 5 | Schemes in which a single photon creates multiple photogenerated carriers. a, Impact ionization, as observed experimentally in most semiconductors at high photon energies. **b**, Multiple exciton generation as found in quantum dots, showing confined energy levels and competing energy-relaxation processes. HOMO, highest occupied molecular orbital; LUMO, lowest unoccupied molecular orbital. **c**, Plot of quantum yield (number of electron–hole pairs created per absorbed photon) as a function of normalized photon energy, for a range of materials, compared with theoretical curves based on the parameter *P* (determined by the relative values of the loss processes in panel **b**). Bulk semiconductors generally have *P* values less than 1, with PbSe nanorods showing the highest values of 7.3 (Si and Ge data from ref. 114; other data from ref. 75). **d,** Limiting energy-conversion efficiency as a function of energy absorption threshold for unconcentrated AM1.5G sunlight across various values of parameter *P*. A value of $P > 10$ is required to improve upon the SQ limits ($P = 0$). Panels **b**–**d** adapted from ref. 75, ACS.

with values over 100 needed for significant gains. Under concentration, small bandgaps become optimal and, consequently, thermodynamic and limiting efficiencies approach those of the thermal devices below[12,77]. A recent milestone[78] demonstrated absolute EQE_{pe} above 100%, although still far below the requirements for worthwhile efficiency gains.

Thermal and related approaches

The earliest approaches for converting sunlight into useful work involved using absorption as heat and subsequent conversion using heat engines[79] (Fig. 6a). The associated thermodynamics are straightforward, particularly under concentrated sunlight, as is normally the case. However, the thermodynamics of several other approaches are very similar, as already noted for multiple-carrier generation, but thermodynamic links also exist to infinite tandem cell stacks, thermophotovoltaics, thermionics and hot carrier cells, which we discuss below.

Solar thermal conversion. As noted, solar thermal conversion involves using heat from a receiver heated to temperature T_C to drive a heat engine, where its performance is limited to the Carnot efficiency $(1 - T_A/T_C)$, where T_A is the ambient temperature. The ideal case can be modelled simply when sunlight is approximated as blackbody radiation characterized by a constant temperature T_S under maximal concentration (46,200 suns). The conversion efficiency limit in this case is:

$$\eta = (1 - T_C^4/T_S^4)(1 - T_A/T_C) \quad (1)$$

The history and properties of this equation are discussed elsewhere[80]. For a 6,000 K Sun and an ambient temperature of 300 K, the optimal efficiency is 85.4% for $T_C = 2{,}544$ K. This receiver temperature is beyond the capability of the materials used in practical solar thermal systems, which are generally limited to $T_C < 1{,}100$ K and efficiencies below 70%, even under the most ideal conditions.

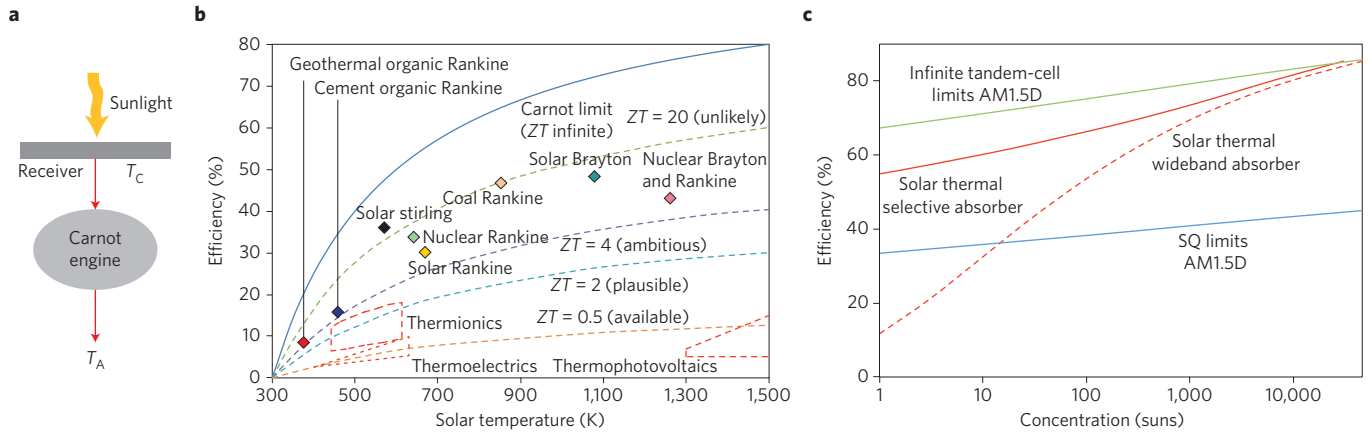

Figure 6 | Solar thermal conversion and conversion efficiencies. a, Idealized solar thermal converter. **b**, Theoretical and experimental conversion efficiencies for converting heat (from a source at the temperature indicated) to electricity, for a range of conversion approaches (sink temperature T_A is 300 K). **c**, Limiting efficiency as a function of sunlight concentration for solar thermal conversion, with and without a selectively absorbing receiver ($T_S = 6{,}000$ K; $T_A = 300$ K), compared with that of an infinite tandem cell and SQ single-junction cell limits, both under concentrated AM1.5D radiation. The thermal limits apply to many of the approaches described in this Review, whereas the infinite tandem results represent upper limits for time-symmetric systems. Panel **b** adapted from ref. 81, Nature Publishing Group, and ref. 82, Annual Reviews.

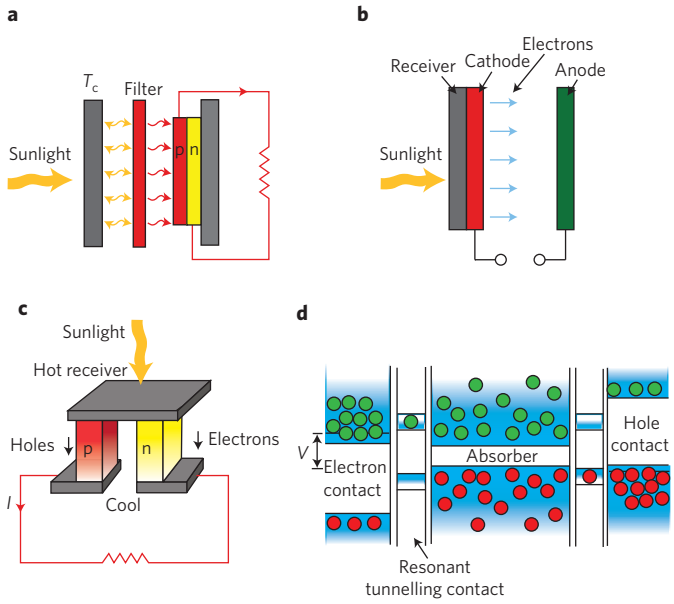

Figure 7 | Approaches that are thermodynamically related to solar thermal conversion. a, Thermophotovoltaics, whereby a cell responds to narrowband optical emission from a solar-heated receiver. **b**, Thermionic conversion, whereby sunlight heats a cathode that emits electrons collected at the cooler anode. **c**, Thermoelectric conversion, whereby a hot receiver produces of flow of carriers towards a cooler junction, thus allowing current flow to be maintained. **d**, Hot-carrier solar cell, in which photogenerated carriers are extracted before relaxing to the absorber band edges. To prevent mixing with cold carriers in the contact, energy-selective contacting is required, as shown using resonant tunnelling contacts in combination with doped semiconductor contact regions.

Figure 6b shows experimental efficiencies for converting heat into electricity from a source at various temperatures, compared with Carnot limits[81,82]. For solar conversion, Stirling engines have the highest experimental values for this stage, with overall solar-to-electricity conversion efficiencies of 31.3% reported[83] and less well-substantiated 34% claimed[84]. Brayton cycles potentially offer higher efficiencies through increased operating temperatures.

However, very high equivalent temperatures can also be reached in ambient-temperature electronic systems owing to exponential increases in carrier excitation, which we noted when discussing SQ limits. The effective emission temperature of electroluminescent light with energy E is not the device temperature T_{dev}, but rather $T_{dev}/(1 - qV/E)$, which becomes high at large internal voltages, V. Consequently, equation (1) also applies to an infinite stack of tandem cells under maximal concentration when all are operated, slightly non-optimally, at a fixed fraction of E_g/q, to give fixed emission temperature[12]. In this case, operation at an effective temperature of 2,544 K poses no thermal problems, which is a fundamental advantage of photovoltaics over solar thermal approaches.

To convert unconcentrated sunlight efficiently, a solar thermal receiver must display energy-selective absorption to avoid excessive radiation back to the Sun. It must strongly absorb high-energy solar photons, but strongly reflect those below a certain threshold to limit thermal emission. Figure 6c shows the similar relationship for limiting efficiency versus concentration ratio for an idealized thermal converter and an infinite tandem cell stack. Although many of the following approaches have limits identical to those of thermal conversion, in experiments they often fall further below the limits seen for practical versus ideal heat engines (Fig. 6b).

Thermophotovoltaics. Thermophotovoltaics is the photovoltaic approach most directly associated with thermal conversion (Fig. 7a). Emission from the heated receiver is confined to a narrow bandwidth, through filtering for example, and directed to a cell. The combination of a narrowband filter and cell acts as an ideal Carnot converter[12], thus giving the same limiting efficiencies as thermal approaches[85]. A passive receiver permits the use of materials with higher receiver temperatures, although experimental solar conversion efficiencies remain modest[86,87], fundamentally due to difficulties associated with designing filters that have the required omnidirectional reflection over the large energy range in which transmission is detrimental.

Recent developments include increased interest in near-field radiative transfer[88], thermophotonics[89] and the closely related 'endothermic conversion'[90], in which the emitter is a heated LED or photoluminescent device. These approaches have inherently narrow-bandwidth emission and can boost emission temperatures by exploiting carrier excitation, as discussed previously.

Thermionics. In thermionics (Fig. 7b), thermal energy is converted to electricity by electrons released at a hot cathode, which are then collected at a cooler anode. This sub-process is limited to the Carnot efficiency, giving an overall limiting performance identical to solar thermal limits. Although thermionic converters have been investigated for powering spacecraft, demonstrated solar conversion efficiencies are below 10% (ref. 91; Fig. 6b).

In the photoelectric effect — the cornerstone of Einstein's Nobel Prize — electrons are ejected from conductors by energetic photons. Sensitive and rapid-response photoelectric photodetectors and photomultipliers have been developed[92], although interest for their use in solar conversion has been modest. The combination of thermionics with photon-enhanced thermionic emission was recently suggested to have potential advantages when high-temperature operation is required[93].

Thermoelectrics. Thermoelectric devices generate voltage when there is a temperature gradient across the junction between two dissimilar conductors, with doped p- and n-type semiconductors being the most effective combination (Fig. 7c). Both electrons and holes migrate from the hot junction, which allows current to flow between the cold terminals. Despite recent improvements in the dimensionless thermoelectric figure-of-merit, the ZT product, which were stimulated by investigations into new materials with high Seebeck coefficients and low thermal but high electrical conductivities[81,82], demonstrated solar conversion efficiencies remain low, generally below 10%. As shown in Fig. 6c, much higher values of the ZT product are required to compete with traditional heat engines[81,82]. Thermodynamically, thermoelectrics has strong links to 'hot carrier cells', which we discuss below.

Hot carrier cells. The loss in excess energy from energetic photons ideally can be avoided by storing this energy in photoexcited carrier populations[94]. This requires slowing the normally rapid relaxation of photogenerated carriers to the bandedge[94–96].

One way to achieve this ideal is to select absorbers with favourable properties for reducing electron-to-phonon energy transfer[95]. A second way is to create 'phonon relaxation bottlenecks' that slow optical phonon relaxation, thereby creating hot phonons[96]. Carrier populations then equilibrate with these hot phonons, rather than with the ambient[96].

Because contacts must allow unrestricted bidirectional carrier interchange for low contact resistance, hot carriers in the absorber would be swamped by cooler contact carriers if interchange between them occurred over the large energy range typical of normal cells. The solution is to allow interchange over a restricted

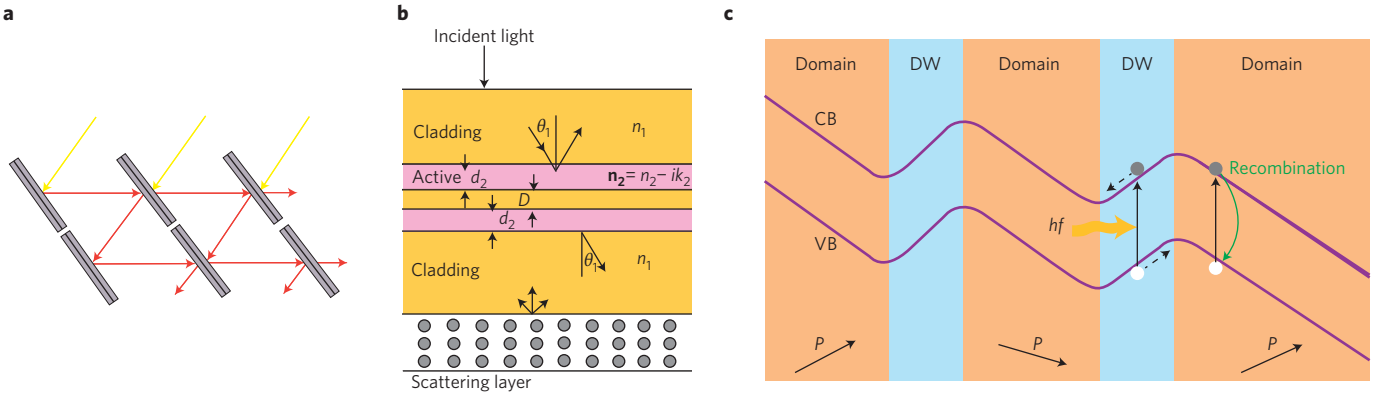

Figure 8 | Alternative high-efficiency approaches. a, Time-asymmetric system with cell emission occurring in a different direction from sunlight incidence, in this restricted acceptance angle implementation. Implementations for diffuse light pose additional challenges[104]. **b**, Absorption enhancement in nanogeometries. The device in this case consists of a nanostructured stack of alternating high-index non-absorbing 'cladding' material and low-index 'active' absorber (n_i and k_i are the real and imaginary parts of the refractive index for the different layers; d_i and D are layer thicknesses; θ_i is the angle of incidence onto the layers shown). **c**, Ferroelectric photovoltaic effect. Change in electric polarization direction (**P**) between different domains induces band-bending across the domain well (DW). *hf* is the photon energy. Panel **c** adapted from ref. 115, Nature Publishing Group.

range[97]. Resonant tunnelling through quantum dots dispersed in a thin dielectric layer between the contact and the absorber may also provide a potential solution[12] by restricting transport to narrow resonant energy ranges (Fig. 7d). Additional heavily doped semiconductors interposed between the dielectric and metal contact (Fig. 7d) can reinforce this selectivity[98]. A balance is needed between the losses that result from excessively wide energy windows and the large contact resistances that result from excessively narrow energy windows[98].

One simple way of maintaining hot carriers is to heat the absorber[99]. The problem then is preventing heat loss to the ambient, which is also the case for thermoelectric devices, indicating some similarities. Geometries similar to Fig. 7d have been suggested for implementing both hot carrier cells and thermoelectric devices[100]. A range of other hot-carrier issues continue to receive theoretical attention. For example, if carriers are all extracted at the same energy, does scattering allow repopulation of the associated states quickly enough to maintain output current[101]?

Although theoretical challenges remain and experimental progress is limited[102], the hot carrier cell remains conceptually attractive as a long-term photovoltaic solution. The two-terminal configuration minimizes interconnection complexity, and ultrathin, strongly absorbing and radiatively efficient cells are essential for reducing material requirements. In addition, hot carrier cells have higher limits than solar thermal conversion and do not require high physical temperatures (subtle band engineering to combine conduction- and valence-band temperatures at each carrier energy allows the ultimate infinite-tandem limit to be reached[103]).

Other approaches

A key limitation — one usually overlooked — is that the SQ approach and developments apply to normal time-symmetric systems, although time symmetry is not an essential photovoltaic device property. Time asymmetry may allow, for example, a cell to absorb light while suppressing the emission that is key to the SQ approach, thereby increasing voltages and efficiencies.

A more detailed study[104] has shown that energy conservation forbids this asymmetry. The best possible result is for cells to emit light in different directions from that received[104]. Emitted light is then available for second-stage conversion, with emission from this stage available for third-stage conversion, and so on (Fig. 8a). Advantages become more pronounced as the efficiency of a single stage increases.

For infinite tandem cells, the time-symmetric efficiency limit under concentrated AM1.5D sunlight is 86.0%. The time-asymmetric limit is 92.8% at ambient temperature[11] (25 °C), but approaches 100% at lower temperatures. The atmospheric window may provide sufficient cooling power to allow the heat dissipated in a cell of this performance (<72 W m^{-2}) to be emitted radiatively into cold space. This would allow operation at temperatures below ambient and thus further boost efficiency, although overall this is an unlikely scenario.

The use of light management[105], such as plasmonics, has been suggested as another way to achieve high efficiencies. Interesting results include the reformulation of light-absorbing limits for thin films using optical densities of states[106], which can be enhanced near interface boundaries (Fig. 8b)[107]. However, SQ limits already assume perfect light absorption; such approaches therefore do not provide paths to exceed SQ limits, but rather provide possibilities for approaching them more closely.

Interest in ferroelectric photovoltaics[108] has been rekindled by the recent emergence of lead-halide perovskite cells[109]. Although the operating principles of these cells are unresolved, ferroelectrics offer above-bandgap voltage output probably by the serial connection of subdomains (Fig. 8c). The efficiencies of such devices remain modest, despite recent improvements[108].

Other recent work combines the techniques described above. This context includes combinations already mentioned, such as photoelectric-enhanced thermionic emission[93], optical hot carrier cells[89,110] and endothermic converters[90], as well as up-converters combined with either down-converters or MEG. Some combinations enhance the prospects for demonstrating practical improvements.

Overall assessment

The present terrestrial photovoltaic manufacturing industry is dominated by silicon cells, and the stranglehold of this technology is tightening[48]. Small, decreasing market shares (<9% combined) are held by CdTe, CIGS and a-Si thin-film modules (including a-Si/nc-Si tandems). For commercial space and concentrator cells, the situation is different owing to different economic trade-offs. In these applications, silicon has been displaced over the past two decades by higher-efficiency GaInP/GaInAs/Ge triple-junction cells, both lattice-matched and metamorphic[111].

Although concentrating photovoltaic cells provide early opportunities for introducing advanced photovoltaics, herein lays a problem, albeit an agreeable one. The improvement rate of III–V

multijunction cells has been the strongest and most sustained of all photovoltaic technologies[6]. Costs, although high, are already close to the requirements of large-scale applications, with further reductions expected as manufacturing volumes increase. Without realistic prospects for efficiencies over 50% and some compelling market advantages, prospects for other advanced concentrator approaches seem to be extremely limited.

Applications in Space may provide other opportunities, not with the aim of replacing III–V multijunctions, but instead for use as thermal converters, through approaches such as thermionics, thermoelectrics and thermophotovoltaics, with such interest contributing to recent development[84]. Ongoing development may lead to other large-scale applications such as the conversion of automobile waste heat, which has been identified as the most likely route for thermoelectrics to contribute to climate-change mitigation[81].

For mainstream terrestrial non-concentrating applications, improved efficiency is key to decreasing important balance-of-system costs[48,112]. Investments in production capacity are huge, and ongoing improvements to silicon technology are restricting the future prospects of emerging technologies[48]. Evolutionary efficiency improvements that are consistent with current manufacturing techniques are therefore the most likely to be adopted. At the opposite extreme, a revolutionary technology that has a compelling efficiency advantage over silicon, while also matching silicon's other attributes, may be capable of displacing it entirely, as is the case for Space and concentrator applications.

The former evolutionary category could include up- and down-conversion cells, and multijunction cells. Up-conversion would be ideal, particularly because cell technology is evolving to make bifacial operation increasingly feasible, although poor up-converter performance constrains prospects. Down-converters could additionally assist with protecting organic encapsulants in conventional modules from ultraviolet light. However, the tandem, series-connected multijunction approach stands out as the strongest candidate for adoption, owing to a better likelihood of actual performance enhancement and scope for ongoing incremental improvements by adding more cells to the stack.

Practical tandem-cell technology is yet to be identified for commercial terrestrial cell technologies, except in the case of a-Si, which has been used in commercial tandem cells for several decades. Peeled III–V films have been of interest, but are expensive. Depositing III–V cells on silicon has been of interest, but the lattice and thermal expansion mismatch has proven problematic for delivering high-performance III–V materials. Promising initial results have been obtained with perovskite/silicon combinations, although poor perovskite stability seems likely to inhibit commercialization. Chalcogenides on silicon have not been widely explored but may provide a solution, if toxic and scarce elements can be avoided. Most tandem technologies developed for silicon would also be of interest for CIGS, given the similarity in bandgaps. The II–VI semiconductor system also offers potential for the development of efficient tandems incorporating CdTe.

In the revolutionary category, the outstanding candidate seems to be the hot carrier cell, for which efficiency limits, with appropriate bandgap engineering[103], can equal that of a tandem stack with an infinite number of cells (Fig. 2c). Although the implementation of an efficient device lies beyond the capability of present technology, ongoing material development may provide solutions to the challenges involved. Devices must be compact and strongly absorbing, with both features consistent with the nano-engineering of the optical density-of-states. Additional control is required over carrier extraction with resonant transport through nanostructures, which is the most likely implementation approach. Decreased electron-to-phonon energy transfer is also essential, with suggested approaches including bandgap or phononic engineering[95,96].

Regardless of the path taken by industry, photovoltaics are now assured to have a major role in the future supply of energy on Earth, with increasing interest in high efficiencies as a way of reducing system costs[112]. Exploiting materials and designs to achieve successful photovoltaic implementations will continue to be an important research area well into the future.

Received 15 February 2016; accepted 23 May 2016; published online 20 December 2016

References

1. Chapin, D. M., Fuller, C. S. & Pearson, G. L. A new silicon p–n junction photocell for converting solar radiation into electrical power. *J. Appl. Phys.* **25,** 676–677 (1954).
2. Prince, M. B. Silicon solar energy converters. *J. Appl. Phys.* **26,** 534–540 (1955).
3. Loferski, J. J. Theoretical considerations governing the choice of the optimum semiconductor for photovoltaic solar energy conversion. *J Appl. Phys.* **27,** 777–784 (1956).
4. Shockley, W. The theory of p–n junctions in semiconductors and p–n junction transistors. *Bell Syst. Tech. J.* **28,** 435–489 (1949).
5. Shockley, W. & Queisser, H. J. Detailed balance limit of efficiency of p–n junction solar cells. *J. Appl. Phys.* **32,** 510–519 (1961).
6. Green, M. A., Emery, K., Hishikawa, Y., Warta, W. & Dunlop, E. D. Solar cell efficiency tables (version 47). *Prog. Photovoltaics* **24,** 3–11 (2016).
7. Green, M. A. Radiative efficiency of state-of-the-art photovoltaic cells. *Prog. Photovoltaics* **20,** 472–476 (2012).
8. Green, M. A. Limits on the open circuit voltage and efficiency of silicon solar cells imposed by intrinsic Auger processes. *IEEE Trans. Electron. Dev.* **ED-31,** 671–678 (1984).
9. Richter, A., Hermle, M. & Glunz, W. Reassessment of the limiting efficiency for crystalline silicon solar cells. *IEEE J. Photovol.* **3,** 1184–1191 (2013).
10. Mattheis, J., Werner, J. H. & Rau, U. Finite mobility effects on the radiative efficiency limit of *pn*-junction solar cells. *Phys. Rev. B* **77,** 085203 (2008).
11. Green, M. A. Limiting photovoltaic efficiency under new ASTM G173 based reference spectra. *Prog. Photovoltaics* **20,** 954–959 (2012).
12. Green, M. A. *Third Generation Photovoltaics: Advanced Solar Energy Conversion* (Springer, 2003).
13. Ross, R. T. Some thermodynamics of photochemical systems. *J. Chem. Phys.* **46,** 4590–4593 (1967).
14. Wurfel, P. The chemical potential of radiation. *J. Phys. C* **15,** 3967–3985 (1982).
15. Green, M. A. Analytical treatment of Trivich–Flinn and Shockley–Queisser photovoltaic efficiency limits using polylogarithms. *Prog. Photovoltaics* **20,** 127–134 (2012).
16. Rau, U. Reciprocity relation between photovoltaic quantum efficiency and electroluminescent emission of solar cells. *Phys. Rev. B* **76,** 085303 (2007).
17. Smestad, G., Ries, H., Winston, R. & Yablonovitch, E. The thermodynamic limits of light concentrators. *Sol. Energ. Mater.* **21,** 99–111 (1990).
18. Carroll, J. J. Global transmissivity and diffuse fraction of solar radiation for clear and cloudy skies as measured and as predicted by bulk transmissivity models. *Sol. Energy* **35,** 105–118 (1985).
19. *Standard Tables for Reference Solar Spectral Irradiances: Direct Normal and Hemispherical on 37° Tilted Surface* ASTM G173–03(2012) (ASTM International, 2012).
20. Campbell, P. & Green, M. A. The limiting efficiency of silicon solar cells under concentrated sunlight. *IEEE Trans. Electron. Dev.* **ED–33,** 234–239 (1986).
21. Araújo, G. L. & Martí, A. Absolute limiting efficiencies for photovoltaic energy conversion. *Sol. Energ. Mater. Sol. C.* **33,** 213–240 (1994).
22. Cornaro, C. & Andreotti, A. Influence of average photon energy index on solar irradiance characteristics and outdoor performance of photovoltaic modules. *Prog. Photovoltaics* **21,** 996–1003 (2013).
23. Hamam, R. E., Celanovic, I. & Soljačić, M. Angular photonic band gap. *Phys. Rev. A* **83,** 035806 (2011).
24. Kosten, E. D., Atwater, J. H., Parsons, J., Polman, A. & Atwater, H. A. Highly efficient GaAs solar cells by limiting light emission angle. *Light Sci. Appl.* **2,** e45 (2013).
25. Höhn, O., Kraus, T., Bauhuis, G., Schwarz, U. T. & Bläsi, B. Maximal power output by solar cells with angular confinement. *Opt. Express* **22,** A715–A722 (2014).
26. Chieng, C. & Green, M. A. Computer simulation of enhanced output from bifacial photovoltaic modules. *Prog. Photovoltaics* **1,** 293–299 (1993).
27. Duran, C., Deuser, H., Harney, R. & Buck, T. Approaches to an improved IV and QE characterization of bifacial silicon solar cells and the prediction of their module performance. *Energy Procedia* **8,** 88–93 (2011).
28. Skoplaki, E. & Palyvos, J. A. Operating temperature of photovoltaic modules: A survey of pertinent correlations. *Renew. Energ.* **34,** 23–29 (2009).

29. Dupré, O., Vaillon, R. & Green, M. A. Physics of the temperature coefficients of solar cells. *Sol. Energ. Mater. Sol. C.* **140,** 92–100 (2015).
30. Raman, A. P., Anoma, M. A., Zhu, L., Rephaeli, E. & Fan, S. Passive radiative cooling below ambient air temperature under direct sunlight. *Nature* **515,** 540–544 (2014).
31. Gentle, A. R. & Smith, G. B. A subambient open roof surface under the mid-summer sun. *Adv. Sci.* **2,** 1500119 (2015).
32. Zhu, L., Raman, A., Wang, K. X., Anoma, M. A. & Fan, S. Radiative cooling of solar cells. *Optica* **1,** 32–38 (2014).
33. Rubin, M. Optical properties of soda lime silica glasses. *Sol. Energ. Mater.* **12,** 275–288 (1985).
34. Zhao, J., Wang, A., Campbell, P. & Green, M. A. 22.7% efficient silicon photovoltaic modules with textured front surface. *IEEE Trans. Electron. Dev.* **46,** 1495–1497 (1999).
35. Jackson, E. D. Areas for improvement of the semiconductor solar energy converter. *Trans. Conf. on the Use of Solar Energy* **5,** 122–126 (1958).
36. Green, M. A. *et al.* 40% efficient sunlight to electricity conversion. *Prog. Photovoltaics* **23,** 685–691 (2015).
37. De Vos, A. Detailed balance limit of the efficiency of tandem solar cells. *J. Phys. D* **13,** 839–846 (1980).
38. Henry, C. H. Limiting efficiencies of ideal single and multiple energy gap terrestrial solar cells. *J. Appl. Phys.* **51,** 4494–4500 (1980).
39. Marti, A & Araujo, G. L. Limiting efficiencies for photovoltaic energy conversion in multigap systems. *Sol. Energ. Mater. Sol. C.* **43,** 203–222 (1996).
40. Chiu, P. T. *et al.* 35.8% space and 38.8% terrestrial 5J direct bonded cells. *Proc. 40th IEEE Photovoltaic Specialist Conf.* 11–13 (2014).
41. Kayes, B. M., Zhang, L., Twist, R., Ding, I. K. & Higashi, G. S. Flexible thin-film tandem solar cells with >30% efficiency. *IEEE J. Photovoltaics* **4,** 729–733 (2014).
42. Takamoto, T. Application of InGaP/GaAs/InGaAs triple junction solar cells to space use and concentrator photovoltaic. *40th IEEE Photovoltaic Specialists Conf.* 1–5 (2014).
43. Sai, H. *et al.* Triple-junction thin-film silicon solar cell fabricated on periodically textured substrate with a stabilized efficiency of 13.6%. *Appl. Phys. Lett.* **106,** 213902 (2014).
44. Matsui, T. *et al.* Development of highly stable and efficient amorphous silicon based solar cells. *Proc. 28th European Photovoltaic Solar Energy Conf.* 2213–2217 (2013).
45. Sai, H. *et al.* High-efficiency microcrystalline silicon solar cells on honeycomb textured substrates grown with high-rate VHF plasma-enhanced chemical vapor deposition. *Jap. J. Appl. Phys.* **54,** 8S1 (2015).
46. New world record for solar cell efficiency at 46% French-German cooperation confirms competitive advantage of European photovoltaic industry *Fraunhofer Institute for Solar Energy Systems* (1 December 2014); http://go.nature.com/2bnQbeA
47. Arvizu, D. E. *Innovation: Enabling a Sustainable Energy Future* (NREL, 2014); http://go.nature.com/2blCoSA
48. Green, M. A. Commercial progress and challenges for photovoltaics. *Nat. Energy* **1,** 15015 (2016).
49. Snaith, H. From nanostructured to thin-film perovskite solar cells. *42nd IEEE Photovoltaic Specialists Conf.* 14–19 (2015).
50. Albrecht, S. *et al.* Monolithic perovskite/silicon-heterojunction tandem solar cells processed at low temperature. *Energ. Environ. Sci.* **9,** 81–88 (2016).
51. Wolf, M. Limitations and possibilities for improvement of photovoltaic solar energy converters. *Proc. IRE* **48,** 1246–1263 (1960).
52. Guttler, G. & Queisser, H. J. Impurity photovoltaic effect in silicon. *Energ. Convers.* **10,** 51–55 (1970).
53. Barnham, K. & Duggan, G. A new approach to high-efficiency multi-band-gap solar cells. *J. Appl. Phys.* **67,** 3490–3493 (1990).
54. Luque, A. & Marti, A. Increasing the efficiency of ideal solar cells by photon induced transitions at intermediate levels. *Phys. Rev. Lett.* **78,** 5014–5017 (1997).
55. Brown, A. S. & Green, M. A. Intermediate band solar cell with many bands: Ideal performance. *J. Appl. Phys.* **94,** 6150–6158 (2003).
56. Luque, A. Thermodynamic consistency of sub-bandgap absorbing solar cell proposals. *IEEE Trans. Electron. Dev.* **48,** 2118–2124 (2001).
57. Ekins-Daukes, N. J. *et al.* High efficiency quantum well solar cells. *24th Workshop on Quantum Solar Energy Conversion* (2012).
58. Brown, A. S. & Green, M. A. Impurity photovoltaic effect: Fundamental energy conversion efficiency limits. *J. Appl. Phys.* **92,** 1329–1336 (2002).
59. Brown, A. S. & Green, M. A. Impurity photovoltaic effect with defect relaxation: Implications for low band gap semiconductors such as silicon. *J. Appl. Phys.* **96,** 2603–2609 (2004).
60. Ramiro, I. & Marti, A. Review of experimental results related to the operation of intermediate band solar cells. *IEEE J. Photovolt.* **4,** 736– 748 (2014).
61. Weber, W. H. & Lambe, J. Luminescent greenhouse collector for solar radiation. *Appl. Opt.* **15,** 2299–2300 (1976).
62. Goetzberger, A. & Greubel, W. Solar energy conversion with fluorescent concentrators. *Appl. Phys.* **14,** 123–129 (1977).
63. Rau, U., Einsele, F. & Glaeser, C. Efficiency limits of photovoltaic fluorescent collectors. *Appl. Phys. Lett.* **87,** 171101 (2005).
64. Richards, B. S., Shalav, A. & Corkish, R. P. A low escape-cone-loss luminescent solar concentrator. *19th Eur. Photovolt. Sol. Energ. Conf.* (2004).
65. Slooff, L. H. *et al.* A luminescent solar concentrator with 7.1% power conversion efficiency. *Phys. Stat. Sol.* **2,** 257–259 (2008).
66. Debije, M. Better luminescent solar panels in prospect. *Nature* **519,** 298–299 (2015).
67. Trupke, T., Green, M. A. & Würfel, P. Improving solar cell efficiencies by the up-conversion of sub-band-gap light. *J. Appl. Phys.* **92,** 4117–4122 (2002).
68. Trupke, T., Shalav, A., Richards, B. S., Wuerfel, P. & Green, M. A. Efficiency enhancement of solar cells by luminescent up-conversion of sunlight. *Sol. Energ. Mater. Sol. C.* **90,** 3327–3338 (2006).
69. Trupke, T. Green, M. A. & Würfel, P. Improving solar cell efficiencies by down-conversion of high-energy photons. *J. Appl. Phys.* **92,** 1668–1674 (2002).
70. Richards, B. S. Luminescent layers for enhanced silicon solar cell performance: Down-conversion. *Sol. Energ. Mater. Sol. C.* **90,** 1189–1207 (2006).
71. Zhang, J. *et al.* Efficient quantum cutting in Tb^{3+}/Yb^{3+} codoped a-$NaYF_4$ single crystals grown by Bridgman method using KF flux for solar photovoltaic. *IEEE J. Quant. Electron.* **51,** 7000206 (2015).
72. Wilkinson, F. J., Farmer, A. J. D. & Geist, J. The near ultraviolet yield of silicon. *J. Appl. Phys.* **54,** 1172–1174 (1983).
73. Deb, S. & Saha, H. Secondary ionisation and its possible bearing on the performance of a solar cell. *Solid State Electron.* **15,** 1389–1391 (1972).
74. Werner, J. H., Brendel, R. & Queisser, H. J. Radiative efficiency limit of terrestrial solar cells. *Appl. Phys. Lett.* **67,** 1028–1030 (1995).
75. Beard, M., Luther, J. M., Semonin, O. & Nozik, A. J. Third generation photovoltaics based on multiple exciton generation in quantum confined semiconductors. *Accounts Chem. Res.* **46,** 1252–1260 (2013).
76. Davis, N. J. L. K. *et al.* Multiple-exciton generation in lead selenide nanorod solar cells with external quantum efficiencies exceeding 120%. *Nat. Commun.* **6,** 8259 (2015).
77. Hanna, M. C., Beard, M. C. & Nozik, A. J. Effect of solar concentration on the thermodynamic power conversion efficiency of quantum dot solar cells. *J. Phys. Chem. Lett.* **3,** 2857–2862 (2012).
78. Semonin, O. E. *et al.* Peak external photocurrent quantum efficiency exceeding 100% via MEG in a quantum dot solar cell. *Science* **334,** 1530–1533 (2011).
79. Perlin, J. *Let It Shine: The 6,000-Year Story of Solar Energy* (New World Library, 2013).
80. Des Vos, A. *Endoreversible thermodynamics of solar energy conversion* (Oxford Univ. Press, 1992).
81. Vining, C. B. An inconvenient truth about thermoelectrics. *Nat. Mater.* **8,** 83–85 (2009).
82. Shakouri, A. Recent developments in semiconductor thermoelectric physics and materials. *Annu. Rev. Mater. Res.* **41,** 399–431 (2011).
83. Stirling Energy Systems set new world record for solar-to-grid conversion efficiency. *Sandia National Laboratories* (12 February 2008); http://go.nature.com/2b2IFAH
84. Barbee, J. Could this be the world's most efficient solar electricity system? *The Guardian* (13 May 2015); http://go.nature.com/2aRxMDa
85. Harder, N.-P. & Würfel, P. Theoretical limits of thermophotovoltaic solar energy conversion. *Semicond. Sci. Tech.* **18,** S151–S157 (2003).
86. Anderson, D. J., Wong, W. A. & Tuttle, K. L. An overview and status of NASA's radioisotope power conversion technology NRA. *Am. Inst. Aero. Astro.* (2005).
87. Ferrari, C., Melino, F., Pinelli, M., Spina, P. R. & Venturini, M. Overview and status of thermophotovoltaic systems. *Energ. Proc.* **45,** 160–169 (2014).
88. Svetovoy, V. B. & Palasantzas, G. Graphene-on-silicon near-field thermophotovoltaic cell. *Phys. Rev. Appl.* **2,** 034006 (2014).
89. Harder, N. & Green, M. A. Thermophotonics. *Semicond. Sci. Tech.* **18,** S270–278 (2003).
90. Manor, A., Martin, L. L. & Rotschild, C. Conservation of photon rate in endothermic photoluminescence and its transition to thermal emission. *Optica* **2,** 585–588 (2015).
91. Habedank, O. D. *Analysis of Topaz II and space-R space nuclear power plants using a modified thermionic model* MSc Thesis, Air Univ. (1993).
92. Yotter, R. A. A review of photodetectors for sensing light-emitting reporters in biological systems. *IEEE Sens. J.* **3,** 288–303 (2003).
93. Schwede, J. W. *et al.* Photon-enhanced thermionic emission for solar concentrator systems. *Nat. Mater.* **9,** 762–767 (2010).
94. Ross, R. T. & Nozik, A. J. Efficiency of hot-carrier solar energy converters. *J. Appl. Phys.* **53,** 3813–3818 (1982).
95. Luque, A. & Marti, A. Electron-phonon energy transfer in hot-carrier solar cells. *Sol. Energ. Mater. Sol. C.* **94,** 287–296 (2010).

96. Conibeer, G. *et al.* Hot carrier solar cell absorber prerequisites and candidate material systems. *Sol. Energ. Mater. Sol. C.* **135,** 124–129 (2015).
97. Wurfel, P. Solar energy conversion with hot electrons from impact ionization. *Sol. Energ. Mater. Sol. C.* **46,** 43–52 (1997).
98. Limpert, S., Bremner, S. & Linke, H. Reversible electron–hole separation in a hot carrier solar cell. *New J. Phys.* **17,** 095004 (2015).
99. Würfel, P. *Solar Olympic Conference* (2000).
100. Humphrey, T. E. & Linke, H. Reversible thermoelectric nanomaterials. *Phys. Rev. Lett.* **94,** 096601 (2005).
101. Takeda, Y. *Quantum Dot Solar Cells* Ch. 8 (eds Wu, J. & Wang, Z. M.) (Springer Science & Business Media, 2013).
102. Dimmock, J. A. R., Day, S., Kauer, M., Smith, K. & Heffernan, J. Demonstration of a hot-carrier photovoltaic cell. *Prog. Photovolt.* **22,** 151–160 (2014).
103. Green, M. Third generation photovoltaics: Recent theoretical progress. *17th Eur. Photovolt. Sol. Energ. Conf.* (2001).
104. Green, M. A. Time-asymmetric photovoltaics. *Nano Lett.* **12,** 5985–5988 (2012).
105. Polman, A. & Atwater, A. Photonic design principles for ultrahigh-efficiency photovoltaics. *Nat. Mater.* **11,** 174–177 (2012).
106. Callahan, D. M., Munday, J. N. & Atwater, H. A. Solar cell light trapping beyond the ray optic limit. *Nano Lett.* **12,** 214–218 (2012).
107. Green, M. A. Enhanced evanescent mode light trapping in organic solar cells and other low index optoelectronic devices. *Prog. Photovolt. Res. Appl.* **19,** 473–477 (2011).
108. Nechache, R. *et al.* Bandgap tuning of multiferroic oxide solar cells. *Nat. Photon.* **9,** 61–67 (2015).
109. Green, M. A., Ho-Baillie, A. & Snaith, H. J. The emergence of perovskite solar cells, *Nat. Photon.* **8,** 506–514 (2014).
110. Farrell, D. J. *et al.* Hot-carrier solar cell with optical energy selective contacts. *Appl. Phys. Lett.* **99,** 111102 (2011).
111. Dimroth, F. High-efficiency solar cells from III–V compound semiconductors. *Phys. Status Solidi C* **3,** 373–379 (2006).
112. *Current and Future Costs of Photovoltaics: Long-term Scenarios for Market Development, System Prices and LCOE of Utility-scale PV Systems* (Fraunhofer Institute for Solar Energy Systems, 2015); http://go.nature.com/2aYJCgc
113. Yoshida, M., Ekins-Daukes, N. J., Farrell, D. J. & Phillips, C. C. Photon ratchet intermediate band solar cells. *Appl. Phys. Lett.* **100,** 263902 (2012).
114. Christensen, O. Quantum efficiency of the internal photoelectric effect in silicon and germanium. *J. Appl. Phys* **47,** 689–695 (1976).
115. Huang, H. Ferroelectric photovoltaics. *Nat. Photon.* **4,** 134–135 (2010).

Acknowledgements

The authors acknowledge support from the Australian Government through the Australian Renewable Energy Agency (ARENA). The Australian Government does not accept responsibility for any information or advice contained herein.

Additional information

Reprints and permission information is available online at www.nature.com/reprints. Correspondence should be addressed to M.A.G.

Competing financial interests

The authors declare no competing financial interests.